Journal of Biomolecular NMR, 4 (1994) 433–454
ESCOM

J-Bio NMR 181

^{1}H, ^{15}N and ^{13}C resonance assignments for the first three zinc fingers of transcription factor IIIA

Xiubei Liao, Karen Clemens, John Cavanagh, Linda Tennant and Peter E. Wright*

Department of Molecular Biology, The Scripps Research Institute, La Jolla, CA 92037, U.S.A.

Received 27 August 1993
Accepted 12 November 1993

Keywords: TFIIIA; Zinc finger; NMR; Structure

SUMMARY

The first three zinc fingers (ZF1–3) of transcription factor IIIA (TFIIIA) from *Xenopus* have been shown to contribute the majority of the binding energy to the intact TFIIIA–DNA interaction [Liao et al. (1992) *J. Mol. Biol.*, **223**, 857–871]. We have expressed a 92-amino acid polypeptide containing the three N-terminal zinc fingers of TFIIIA. This three-fingered polypeptide has been isotopically labeled with ^{15}N and ^{13}C in *E. coli* and purified to homogeneity. Assignment of backbone ^{1}H,^{15}N, aliphatic ^{1}H and ^{13}C and aromatic ^{1}H and ^{13}C resonances of ΔNZF1–3 has been obtained using a combination of single-, double- and triple-resonance multidimensional NMR experiments. The secondary structures for each finger have been determined from NOE connectivities, $^{3}J_{NH\alpha}$ values and chemical shifts. The results show that each finger folds into a canonical β-sheet-helix zinc finger structural motif, while the linkers adopt an extended structure. The helix between the two histidine ligands in ZF3 is distorted by zinc coordination, to accommodate the presence of four intervening amino acids instead of three as in ZF1 and ZF2.

INTRODUCTION

The 5S RNA gene-specific transcription factor IIIA (TFIIIA) from *Xenopus* contains a nucleic acid-binding domain, consisting of nine Cys_2-His_2 zinc fingers (Engelke et al., 1980; Ginsberg et al., 1984; Smith et al., 1984; Miller et al., 1985; Vrana et al., 1988). It has been shown that the zinc fingers of TFIIIA bind both to the internal control region (ICR) of the 5S RNA gene and to the 5S RNA gene product, a property which is unique to this transcription factor (Engelke et al., 1980; Honda and Roeder, 1980; Pelham and Brown, 1980; Sakonju et al., 1980; Clemens et al., 1993). Previous studies demonstrated that the three N-terminal fingers (ZF1–3) of TFIIIA bind specifically to the 3' end of the ICR region of the 5S RNA gene and contribute the majority of binding energy of the TFIII–DNA interaction (Liao et al., 1992).

Since the Cys_2-His_2-type zinc finger motif has been found in many nucleic acid-binding proteins

*To whom correspondence should be addressed.

(El-Baradi and Pieler, 1991), great interest in the structures of these zinc fingers and their DNA complexes has developed. The first 3D structure of an individual finger domain resulted from an NMR study of a Cys_2-His_2 zinc finger from the *Xenopus* protein Xfin (Lee et al., 1989). Later, the structures of several single and double Cys_2-His_2 zinc finger polypeptides were solved by high-resolution NMR techniques; these include the human male-associated protein ZFY (Kochoyan et al., 1991a,b), the yeast protein ADR1 (Klevit et al., 1991) and the human HIV-1 enhancer binding protein (Omichinski et al., 1990,1992). The fingers of each of these polypeptides fold into a canonical structure which contains an antiparallel β-hairpin, followed by a short amphipathic helix. The two conserved cysteine residues near the turn of the β-sheet and two invariable histidines near the C-terminus of the helix coordinate a central zinc ion; metal coordination allows each finger to fold into a compact globular domain, stabilized by hydrophobic interactions. The crystallographic structure of a DNA complex of three zinc fingers from the eukaryotic regulatory protein zif268 provides further detailed information on the zinc finger fold (Pavletich and Pabo, 1991). These results clearly show that the 3D structure is preserved in the DNA complex.

The fact that zinc finger proteins generally contain multiple copies of finger domains (El-Baradi and Pieler, 1991) poses two important questions: (i) are the domains independent or do they interact with each other; and (ii) is the zinc finger–nucleic acid interaction dependent on interdomain interactions. In order to fully understand the mechanism of zinc finger–nucleic acid interactions, it is necessary to study the structure of multifinger domains both free and complexed to DNA.

Homonuclear multidimensional NMR techniques have been used successfully to obtain structures of a number of proteins of less than 10 kDa (Bax, 1989; Clore and Gronenborn, 1989; Wüthrich, 1986,1989). However, the similarities in the structures of fingers previously determined indicate that homonuclear techniques alone may not be sufficient to study a protein containing multiple zinc fingers, due to the expected resonance overlap. Recent progress in heteronuclear multidimensional NMR has allowed great improvement in the spectral quality of large proteins (Fesik and Zuiderweg, 1990; McIntosh and Dahlquist, 1990). This methodology was used for the current investigation of a multifingered protein. These techniques label at least one spectral dimension with ^{15}N or ^{13}C chemical shifts, and the generally larger chemical shift dispersion of the heteronuclear resonances aids in the resolution of many ambiguities found in homonuclear 2D and 3D experiments.

In this paper, the ^{1}H, ^{15}N and ^{13}C assignments of a protein containing the first three fingers

---

Abbreviations: TFIIIA, transcription factor IIIA; ZF1, ZF2, ZF3, zinc finger 1, 2, 3; ZF1-3, zinc fingers 1 to 3; 2D, 3D, 4D, two-, three-, four-dimensional; 2Q, double-quantum spectroscopy; HCA(CO)N, 3D triple-resonance $^{1}H^{\alpha}$-$^{13}C^{\alpha}$-^{15}N correlation spectroscopy; ^{1}H-^{13}C HMQC-NOESY-HMQC, 4D heteronuclear ^{1}H-^{13}C multiple-quantum coherence ^{1}H nuclear Overhauser ^{1}H-^{13}C multiple-quantum coherence spectroscopy; HSQC, heteronuclear single-quantum coherence spectroscopy; ^{1}H-^{13}C NOESY-HSQC, 3D heteronuclear ^{1}H nuclear Overhauser ^{1}H-^{13}C single-quantum coherence spectroscopy; ^{1}H-^{15}N NOESY-HSQC, 3D heteronuclear ^{1}H nuclear Overhauser ^{1}H-^{15}N single-quantum coherence spectroscopy; ^{1}H-^{15}N SE.TOCSY-HMQC, 3D sensitivity-enhanced heteronuclear ^{1}H total correlation ^{1}H-^{15}N multiple-quantum coherence spectroscopy; ^{1}H-^{15}N TOCSY-HSQC, 3D heteronuclear ^{1}H total correlation ^{1}H-^{15}N single-quantum coherence spectroscopy; HCCH-COSY, 3D ^{1}H-^{13}C-^{13}C-^{1}H correlation spectroscopy via $^{1}J_{CC}$ coupling; HCCH-TOCSY, 3D ^{1}H-^{13}C-^{13}C-^{1}H total correlation spectroscopy via isotropic mixing of ^{13}C magnetization; NOE, nuclear Overhauser effect; NOESY, nuclear Overhauser enhancement spectroscopy; SL, spin-lock purge pulse; TMS, tetramethylsilane; TOCSY, total correlation spectroscopy; TPPI, time-proportional phase incrementation.

Fig. 1. The amino acid sequence of ΔNZF1–3 in the one-letter code. The numbering of each finger is given at the top. The S in parentheses represents the cysteine-to-serine replacement.

(ΔNZF1–3) of TFIIIA from *Xenopus* are described. This construct carries a nonessential cysteine-to-serine substitution in the first finger and a deletion of the hydrophobic N-terminal residues 2–10. The spectra of ΔNZF1–3 are dramatically improved by these mutations and the DNA-binding properties of ΔNZF1–3 are unchanged from those of the wild-type ZF1–3 (Clemens et al., 1992). The backbone resonance assignments of ΔNZF1–3 were obtained using ^{1}H-^{15}N-correlated 3D experiments, where the improved dispersion of ^{15}N chemical shifts helped to unambiguously assign the overlapped NH and $C^{\alpha}H$ protons. The resonance assignments of aliphatic side chains were based on ^{1}H-^{13}C-correlated HCCH-TOCSY and HCCH-COSY 3D experiments, which transfer magnetization efficiently via the uniformly large $^{1}J_{CC}$ couplings. The backbone assignments and the side-chain assignments were further confirmed by a ^{1}H-^{13}C-^{15}N HCA(CO)N triple-resonance experiment. The secondary structure of ΔNZF1–3 was determined from the NMR data. The structural motif and chemical shifts of each finger are compared.

This is the first NMR study of a three-fingered protein which binds DNA with high sequence specificity. The assignments and structural studies of ΔNZF1–3 provide a starting point to study the spatial relationship among fingers in a multifingered protein and to elucidate the structure of the complex of ΔNZF1–3 with DNA.

MATERIALS AND METHODS

Protein sequence and numbering of ΔNZF1–3

The ΔNZF1–3 sequence is shown in Fig. 1. The S in parentheses represents the replacement of the wild-type cysteine of ZF1–3 with serine. The amino acid sequence is numbered such that the first conserved aromatic residue of each finger is x01 (where x = 1, 2, 3 for ZF1, ZF2, and ZF3, respectively). ZF1 consists of Tyr^{101} through Pro^{130}, which includes the linker between ZF1 and ZF2; Phe^{201} through Asn^{230} represent ZF2 and the subsequent linker; and Phe^{301} through Lys^{329} contain ZF3 and part of the linker following ZF3. Three residues precede ZF1 in the construct, and are designated Met^{98}, Lys^{99} and Arg^{100}. The advantage of this numbering scheme is that the conserved residues in each finger can be easily identified, for example, Cys^{103}, Cys^{203} and Cys^{303} represent the first conserved cysteine ligand in each finger. Note, however, that the second

conserved histidine is His^{125} and His^{225} for ZF1 and ZF2 respectively, but His^{326} for ZF3, due to the insertion of a fourth residue between the histidine ligands in this finger.

Expression of ΔNZF1–3 and purification from inclusion bodies

The gene construction of ΔNZF1–3 was described previously (Clemens et al., 1992; Liao et al., 1992). Unlabeled ΔNZF1–3 was produced in *E. coli* BL21-DE3(PlysS) by induction of T7 polymerase at mid-log growth in LB media, with addition of IPTG to 0.5 mM. Uniformly labeled ΔNZF1–3 was produced by growth in isotopically enriched minimal medium (0.6% Na_2HPO_4, 0.3% KH_2PO_4, 0.15% NaCl, 1 mM $MgCl_2$ and 0.1 mM $CaCl_2$), containing either 1.5 g/l $(^{15}NH_4)_2SO_4$ and 2 g/l of ^{13}C glucose for double labeling, or 1 g/l $(^{15}NH_4)_2SO_4$ and 4 g/l of unlabeled glucose for ^{15}N labeling. Protein expression in minimal media was induced at an OD_{600} of ~ 0.8 and cells were grown for six more hours at 37 °C. Cells from either rich media or minimal media were collected by centrifugation at 5000 g for 10 min. The cell pellet was resuspended in lysis buffer (50 mM phosphate (pH 6.5), 5 mM DTT, 150 mM NaCl, 50 μM $ZnCl_2$). After brief sonication, inclusion bodies were pelleted by centrifugation at 28 000 g for 20 min at 4 °C. The insoluble ΔNZF1–3 was suspended in solubilizing buffer (50 mM phosphate (pH 6.5), 20 mM DTT, 150 mM NaCl, 200 μM $ZnCl_2$ and 5 M urea) and solubilized by sonication and vigorous shaking for 30 min. The supernatant was loaded directly onto a heparin-Sepharose column, prewashed with the low-salt lysis buffer and the ΔNZF1–3 was eluted with a 0.15–1 M NaCl gradient. Fractions were analyzed by silver-stained SDS-page. The fractions containing ΔNZF1–3 were pooled and concentrated by ultrafiltration. Residual contaminants and salt were removed by passing the concentrated fraction through a Superdex column (Pharmacia), equilibrated with low-salt buffer (30 mM phosphate (pH 6.5), 30 mM NaCl, 5 mM DTT, 50 μM $ZnCl_2$). The pooled fraction ran as a single band on SDS-page. The ΔNZF1–3 had the expected N-terminal sequence, the correct molecular mass by ion spray mass spectrometry, and was fully active in DNA binding assays (Clemens et al., 1992).

NMR sample preparation

The purified ΔNZF1–3 was exchanged into NMR buffer (30 mM phosphate (pH 6.5), 30 mM NaCl, 5 mM deuterated DTT, 50 μM $ZnCl_2$) in either 99.99% D_2O or 10% D_2O/90% H_2O by ultrafiltration and then saturated with argon in the NMR tube. The concentration of ΔNZF1–3 for NMR studies was 0.5–0.8 mM. Precipitation was observed when the concentration of ΔNZF1–3 was higher than 1 mM. Fluorescence studies, NMR relaxation measurements and concentration dependence measurements indicated that ΔNZF1–3 is monomeric in solution, even at NMR concentration (Liao et al., unpublished results). NMR samples were stored at 4 °C.

NMR methods

NMR spectra were recorded on Bruker AMX 500 or AMX 600 spectrometers at 300 K. Proton chemical shifts were referenced to TMS. The ^{15}N and ^{13}C chemical shifts were indirectly referenced to NH_3 and TMS, using the $^{15}N/^1H$ frequency ratio of 0.1013291444 (Live et al., 1984) and the $^{13}C/^1H$ frequency ratio of 0.25145002 (Bax and Subramanian, 1986). Uncertainties in the reported chemical shifts are 0.02, 0.3 and 0.1 ppm for ^1H, ^{13}C and ^{15}N, respectively.

Homonuclear double-quantum (2Q) (Braunschweiler et al., 1984; Rance and Wright, 1986), TOCSY (Braunschweiler and Ernst, 1983) and NOESY (Jeener et al., 1979) spectra were record-

ed in D_2O at 300 K. The residual H_2O resonance was suppressed using a low-power presaturation pulse. A 40-ms double-quantum coherence preparation period was used in the 2Q experiment; a 52.6-ms DIPSI-2 isotropic mixing sequence (Shaka et al., 1988) was used in the homonuclear TOCSY experiment and a 110-ms mixing time was used in the NOESY experiment. The carrier was set on the residual H_2O resonance and TPPI was used for frequency discrimination in F_1 in all 2D experiments (Marion and Wüthrich, 1983). Spectra were acquired with a spectral width of 12500 Hz and 4K complex points in the F_2 dimension, 512 t_1 increments in homonuclear TOCSY and NOESY experiments (spectral width 5681.8 Hz) and 800 t_1 increments in the 2Q experiment (spectral width 10330.6 Hz).

The 2D ^1H-^{15}N-correlated HSQC spectrum (Bodenhausen and Ruben, 1980) and 3D ^1H-^{15}N-correlated SE.TOCSY-HMQC, TOCSY-HSQC(SL), NOESY-HSQC and NOESY-HSQC(SL) spectra were acquired as described elsewhere (Bax et al., 1990a; Norwood et al., 1990; Palmer et al., 1991) in 90% H_2O/10% D_2O. GARP-1 decoupling (Shaka et al., 1985) was applied during the detection period of all heteronuclear multidimensional experiments. The SE.TOCSY-HMQC experiment employs the sensitivity-improved TOCSY scheme (Cavanagh and Rance, 1990; Palmer et al., 1991). Both low-power H_2O irradiation (SE.TOCSY-HMQC and NOESY-HSQC) and spin-lock purge pulses (TOCSY-HSQC(SL) and NOESY-HSQC(SL)) were used for suppression of the H_2O signal (Messerle et al., 1989). The 2D HSQC spectrum (Bodenhausen and Ruben, 1980) was acquired with 4K complex points in the F_2 proton dimension and 450 increments in the F_1 ^{15}N dimension. The spectral widths were 2427.3 and 12500.0 Hz in F_1 and F_2, respectively. The carrier frequencies were at the H_2O resonance in F_2 and at 116.0 ppm in the F_1 ^{15}N dimension. All 3D ^1H-^{15}N-correlated experiments were recorded in the phase-sensitive mode using TPPI in both the F_1 and F_2 dimensions (Marion and Wüthrich, 1983). Spectra were acquired with 512 complex points in F_3, 256 increments in F_1 and 64 increments in the F_2 dimension. The spectral widths were 6097.6, 9259.3 and 1545.1 Hz in the F_1,F_3 proton dimensions and the F_2 ^{15}N dimension, respectively. The carrier frequency was placed at the H_2O resonance in the F_1 and F_3 proton dimensions and at 120.5 ppm in the F_2 ^{15}N dimension.

A J-coupling-modulated HSQC experiment was performed as described by Neri et al. (1990), but with addition of a refocussed INEPT sequence (Morris and Freeman, 1979) before acquisition, to generate in-phase correlation peaks in the F_2 dimension. Spectra were recorded with a spectral width of 9090.9 Hz and 2K complex data points in the F_2 proton dimension, and with a spectral width of 1165.0 Hz and 400 increments in the F_1 ^{15}N dimension. A total of 13 J-modulated HSQC experiments were recorded with delays ranging from 3 μs to 160 ms. Peak heights were measured using an in-house written FORTRAN routine. Experimental data were fit to the equation $I = I_o\cos(3.142 \times {}^3J_{HN\alpha} \times t)\exp(-ct)$, where c is the time constant for antiphase T_2 ($S_zI_{x,y}$) relaxation in the J modulation period.

All HCCH experiments were recorded in D_2O. The HCCH-TOCSY experiment was performed as described previously (Bax et al., 1990b). A 21.2-ms DIPSI-2 sequence (10 kHz) was used for the isotropic mixing period and the carbonyl inversion pulse was applied on-resonance. The constant-time HCCH-COSY experiment was performed using the published scheme of Ikura et al. (1991). The ^1H-^{13}C-correlated 3D NOESY-HSQC experiment was performed using a 100-ms mixing time. The ^1H and ^{13}C carriers were placed at 2.06 and 41.4 ppm, respectively. Quadrature detection in t_1 and t_2 was achieved using the TPPI-States and States methods, respectively (Marion et al., 1989). The data matrix contained $128 \times 32 \times 512$ complex data points in the

$F_1 \times F_2 \times F_3$ dimensions. The spectral widths were 4000.0, 12500.0 and 4843.8 Hz in the F_1,F_3 proton dimensions and F_2 ^{13}C dimension, respectively.

The 4D ^1H-^{13}C-correlated HMQC-NOESY-HMQC experiment was performed according to the pulse sequence of Clore et al. (1991) with a 100-ms mixing time. The ^1H carrier was placed at 3.20 ppm and the centers for the two ^{13}C dimensions were set at 41.4 ppm. Frequency discrimination was achieved using the States method in the t_1 and t_3 periods, and TPPI-States in the t_2 period. The data matrix contained $8 \times 64 \times 8 \times 256$ complex data points in the $F_1 \times F_2 \times F_3 \times F_4$ dimensions, respectively. The spectral widths were 4807.7 and 6250.0 Hz in the F_2 and F_4 proton dimensions and 4845.4 kHz in the F_1 and F_3 carbon dimensions.

The 2D ^1H-^{13}C-correlated HSQC spectrum of the aromatic region was acquired with the ^{13}C carrier at 126.0 ppm and the ^1H carrier at the residual H_2O resonance. The spectrum was acquired with 4K complex points in the F_2 dimension and 330 increments in t_1. The spectral widths were 2415.5 Hz in the F_1 carbon dimension and 12500.0 Hz in the F_2 proton dimension.

The 3D constant-time HCA(CO)N experiment was performed as described by Palmer et al. (1992). The ^1H, aliphatic ^{13}C and ^{15}N pulses were generated using the three spectrometer rf channels. Carbonyl ^{13}C pulses were generated using a home-built fourth channel. The TPPI-States method was used for F_1 and F_2 frequency discrimination (Marion et al., 1989). The spectral widths were 3333.3 Hz in the F_1 ^{13}C dimension, 1926.8 Hz in the F_2 ^{15}N dimension and 12500.0 Hz in the F_3 ^1H dimension. The data matrix consisted of $58 \times 32 \times 512$ complex points, respectively. The ^1H carrier was placed at the residual H_2O resonance (4.74 ppm), the ^{15}N carrier at 119.0 ppm and the ^{13}C carrier at 52.5 ppm.

Data for 2D and 3D experiments were processed on either a CONVEX C240 or a SUN SPARC workstation, using a modified version of the FTNMR software (Hare Research, Inc.). The F_2 dimension in 3D spectra was generated using in-house FORTRAN routines. Data for the 4D spectrum were processed on a SPARC workstation, using the FELIX 2.05 software (Hare Research, Inc.).

RESULTS AND DISCUSSION

Resonance assignments

ΔNZF1–3 contains three Cys_2-His_2 zinc fingers and a total of 92 amino acids. Figure 2 shows the ^1H-^{15}N HSQC spectrum of ΔNZF1–3 with the assignments of the cross peaks indicated. The spectrum is well resolved and contains 80 ^1H-^{15}N cross peaks out of the 89 backbone amide resonances expected; the missing peaks are due to amide exchange with the solvent. Four of the exchanging amide resonances, Gly^{307}, Glu^{209}, Thr^{213} and Thr^{313}, can be observed in 3D ^1H-^{15}N-correlated spectra and 2D ^1H-^{15}N HSQC spectra when spin-lock purge pulses are used for suppression of the H_2O resonance. ^1H-^{15}N cross peaks missing from these spectra are those of Lys^{99}, the second amino acid from the N-terminus, and Asn^{113}, Asn^{115}, Trp^{116} and His^{216} which are amino acid residues located in the regions linking the β-sheet and the helix in ZF1 and ZF2. These five ^1H-^{15}N resonances could not be unambiguously detected in any of the ^1H-^{15}N-correlated spectra; the amides may be in very rapid exchange with H_2O protons, on a time scale comparable to the length of the pulse sequences. The HSQC spectrum also contains well-resolved pairs of ^1H-^{15}N cross peaks for five of the seven side chains of asparagine and glutamine residues. These peaks can be easily distinguished from backbone amide peaks by the weak ^{15}NHD 'tail', observed

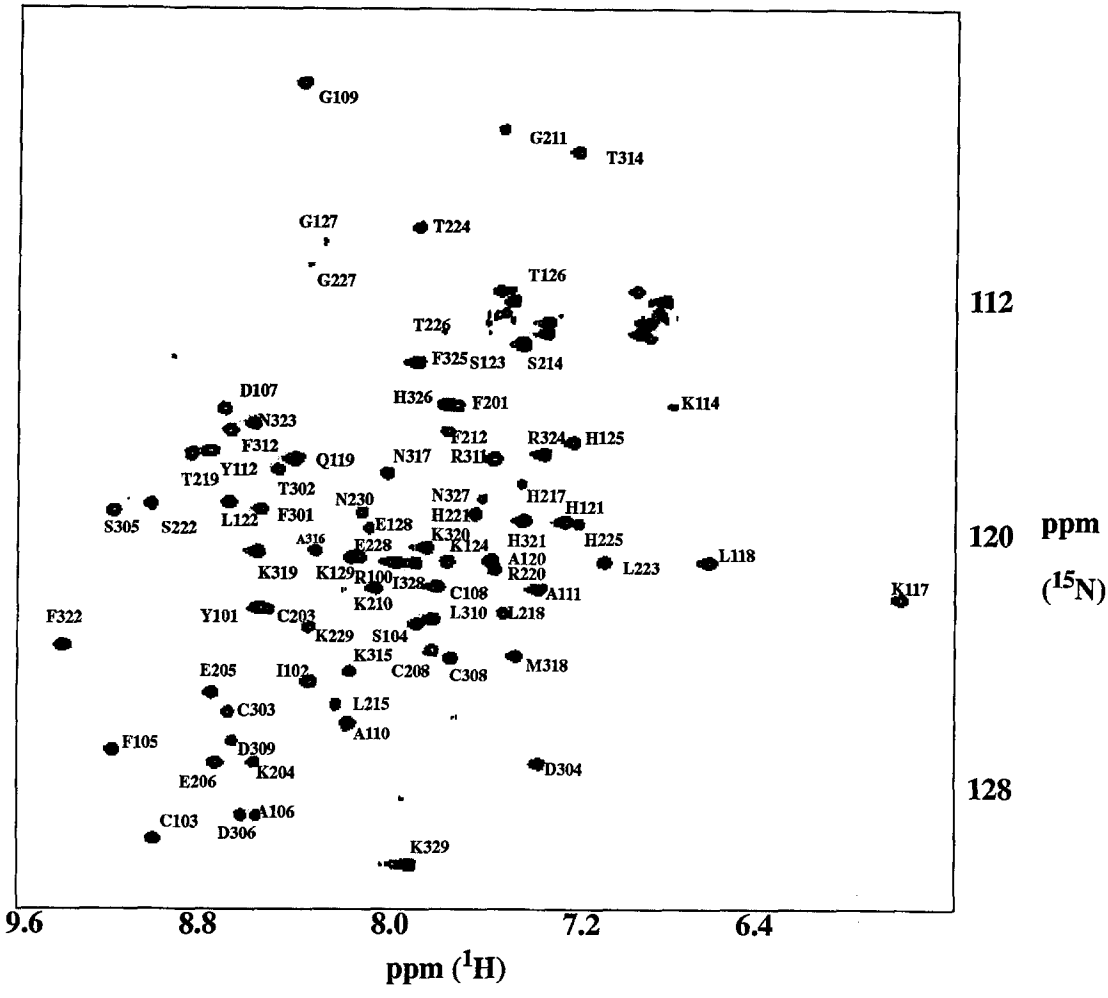

Fig. 2. ^{1}H-^{15}N HSQC spectrum of uniformly ^{15}N-labeled ΔNZF1–3 recorded at 600 MHz, pH 6.5, 300 K. The assignments obtained in this study are indicated.

upfield from the main peaks and their chemical shifts (110–115 ppm) in the ^{15}N dimension. The ^{1}H-^{15}N cross peaks from glycine and threonine usually have the most upfield chemical shifts in the ^{15}N dimension, and can be used as convenient starting points for sequential assignment. In some ^{1}H-^{15}N-correlated spectra, several weak cross peaks from a minor conformation of ZF1 were observed. This minor form can be removed by HPLC purification (Clemens et al., unpublished results).

Heteronuclear 3D techniques further increase spectral resolution, compared to 2D techniques. Like their 2D homologues, the 3D TOCSY spectrum is used to identify the individual spin systems and 3D NOESY is used to identify the connectivities between residues. The backbone ^{15}N and ^{1}H assignments of ΔNZF1–3 were based on the systematic analysis of 3D SE.TOCSY-HMQC, NOESY-HSQC, 3D TOCSY-HSQC(SL) and 3D NOESY-HSQC(SL) spectra. Using spin-lock purge pulses for suppression of the H_2O resonance (Messerle et al., 1989), 3D TOCSY-

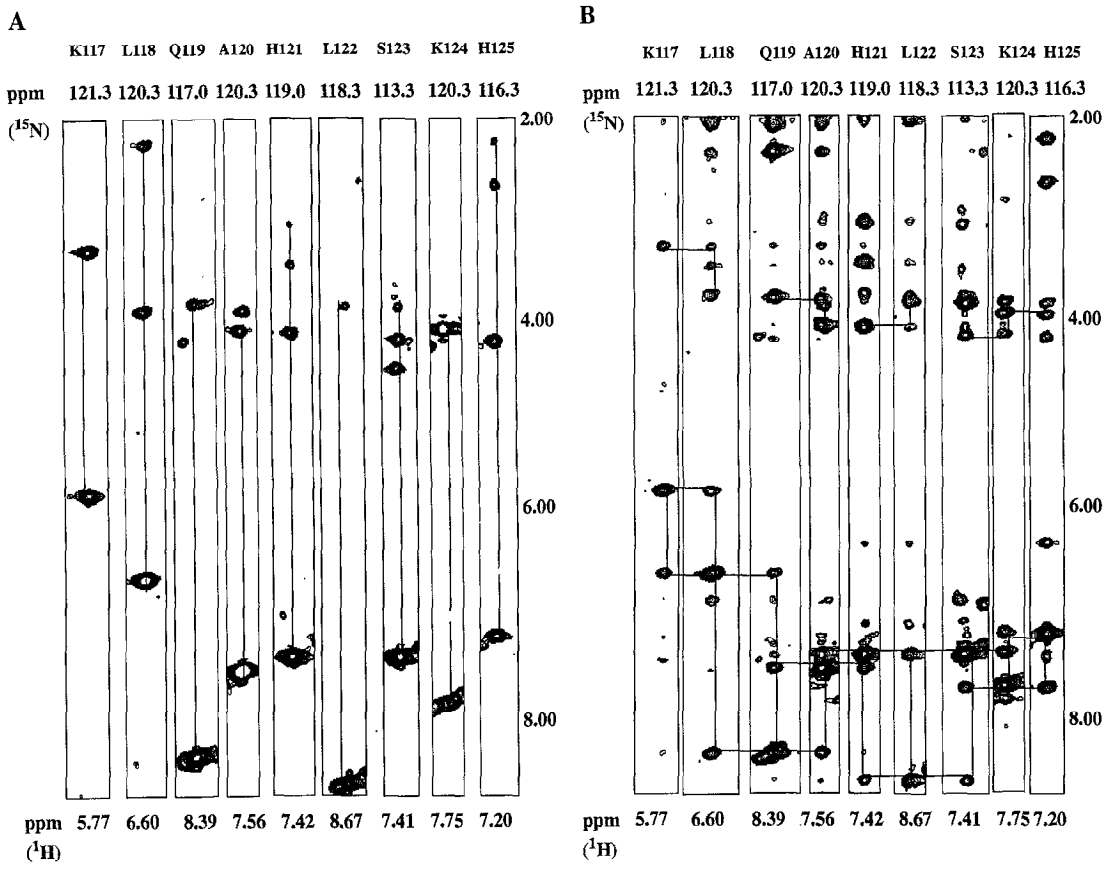

Fig. 3. (A) Strips taken from the amide region of different ^{15}N planes of the 3D SE.TOCSY-HMQC spectrum of ΔNZF1–3, arranged in sequential order for residues Lys^{117} to His^{125}. The ^{15}N chemical shift and sequential assignment are indicated at the top and the amide ^{1}H chemical shift is shown at the bottom of each strip. A line is drawn between the diagonal H^N peaks and corresponding NH-$C^{\alpha}H$ and NH-$C^{\beta}H$ cross peaks. (B) The corresponding amide strips from the 3D NOESY-HSQC spectrum of ΔNZF1–3. Sequential $d_{\alpha N}(i,i+1)$ and $d_{NN}(i,i+1)$ NOE connectivities are indicated by solid lines.

HSQC(SL) and NOESY-HSQC(SL) experiments allow recovery of some labile amide resonances and $C^{\alpha}H$ resonances which are bleached by solvent irradiation in the SE.TOCSY-HMQC and NOESY-HSQC spectra. Short-range NOE cross peaks were used to connect individual spin systems to obtain sequential assignments. Figure 3 illustrates the sequential assignment of residues 117–125 in ZF1. Figure 3A contains slices selected from the 3D SE.TOCSY-HMQC spectrum at different ^{15}N chemical shifts. Starting from the F_1–F_3 amide peaks, the through-bond connectivities are linked on each slice. Figure 3B presents corresponding slices, selected from the 3D NOESY-HSQC spectrum; the $d_{NN}(i,i+1)$ and $d_{\alpha N}(i,i+1)$ NOE connectivities used for sequential assignment are linked by solid lines. The strong $d_{NN}(i,i+1)$ connectivities in Fig. 3B suggest that residues 119–128 form a helical structure.

While ^{1}H-^{15}N-correlated heteronuclear 3D spectra provided the majority of the backbone assignments, these experiments were not sufficient to obtain complete assignments. An isotropic

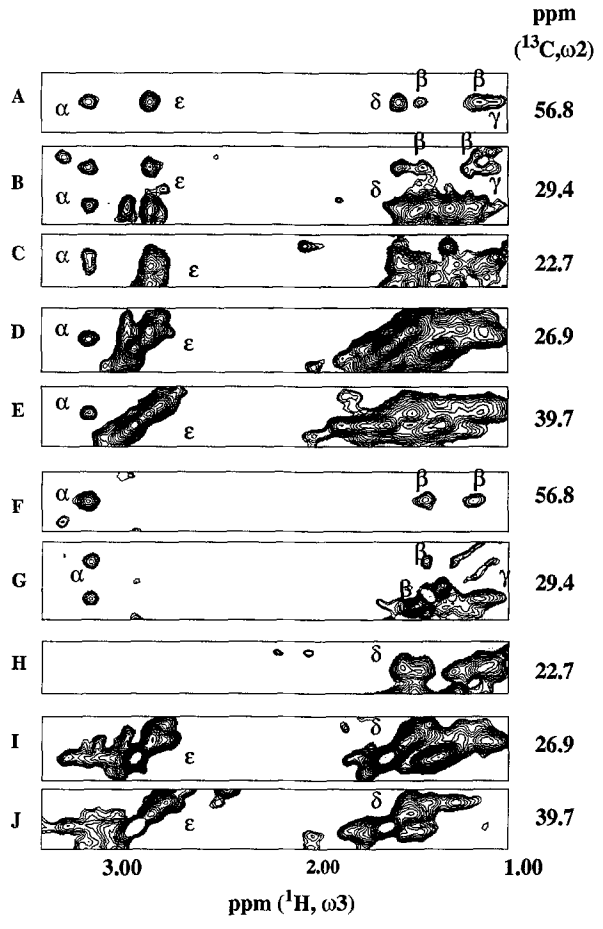

Fig. 4. Slices from the 3D HCCH-TOCSY (A–E) and 3D HCCH-COSY (F–J) spectra of uniformly ^{15}N, ^{13}C-labeled ΔNZF1–3, demonstrating the assignment of Lys^{315}. The ^{13}C chemical shifts of corresponding resonances are indicated on the right.

mixing period of 40 ms provided the best overall results in the ^{1}H-^{15}N-correlated SE.TOCSY-HMQC and TOCSY-HSQC experiments. However, with this short mixing period, most of the $C^{\gamma}H$, $C^{\delta}H$ and $C^{\varepsilon}H$ to NH cross peaks are absent, due to small $^{3}J_{HH}$ coupling constants. In order to overcome this problem and obtain unambiguous aliphatic side-chain assignments, ^{1}H-^{13}C-correlated 3D HCCH-TOCSY and 3D constant-time HCCH-COSY experiments were performed.

In HCCH-type experiments, ^{1}H magnetization is transferred to the directly attached ^{13}C, then the carbon magnetization is transferred through the ^{13}C spin network. Finally, ^{13}C magnetization is transferred back to the directly attached ^{1}H for detection. Since $^{1}J_{HC}$ and $^{1}J_{CC}$ are both large (~140 Hz for $^{1}J_{HC}$ and ~40 Hz for $^{1}J_{CC}$), a short 22.5-ms isotropic mixing period was optimal for efficient magnetization transfer in the HCCH-TOCSY experiment. For side chains of A_3X, AX and AMX spin systems, resonances were identified in either HCCH-TOCSY or HCCH-COSY spectra. For side chains of longer spin systems, difficulties were often encountered with chemical

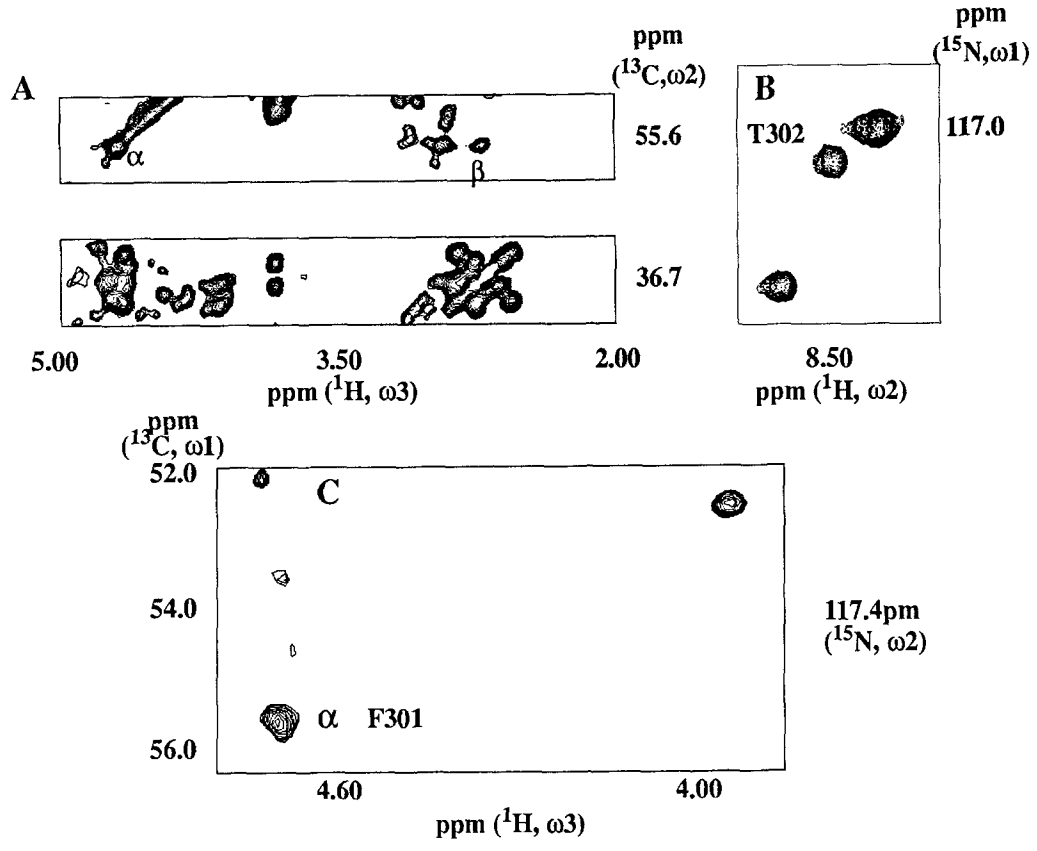

Fig. 5. Sections from (A) 3D ^{1}H-^{13}C-correlated HCCH-COSY; (B) ^{1}H-^{15}N-correlated HSQC; and (C) ^{1}H-^{13}C-^{15}N-correlated HCA(CO)N spectra, illustrating the assignment of the through-bond connectivity between Phe^{301} and Thr^{302}.

shift overlap among β, γ and δ resonances. By combining HCCH-TOCSY and HCCH-COSY spectra, the overlap among β, γ and δ resonances could be resolved for most long side chains. This is illustrated in Fig. 4, which shows slices from the HCCH-TOCSY (A–E) and HCCH-COSY (F–J) experiments at different ^{13}C chemical shifts of the Lys^{315} side chain. Figures 4A and 4F show that, starting from C$^{\alpha}$, the magnetization is transferred to C$^{\varepsilon}$ in the HCCH-TOCSY experiment, but only reaches C$^{\beta}$ in the HCCH-COSY experiment. Thus, β, γ and δ resonances of Lys^{315} can be unambiguously distinguished.

Since the aromatic side chains provide the hydrophobic core of the zinc finger domain (Lee et al., 1989), assignment of aromatic side chains is crucial for tertiary structural determination of ΔNZF1–3. The chemical shifts of aromatic ring carbons, which range from 115 to 135 ppm, are more than 70 ppm away from the chemical shifts of aliphatic carbons. The 3D HCCH-TOCSY experiment cannot be used to transfer coherence between aliphatic carbons and aromatic carbons due to this large frequency difference, which is greater than the bandwidth of the DIPSI-2 mixing sequence. Aromatic resonance assignments were made using homonuclear double-quantum (2Q), TOCSY and NOESY and ^{1}H-^{13}C-correlated HSQC spectra of ΔNZF1–3 in D_2O. The amide resonances, which are partially overlapped with the aromatic proton resonances, were

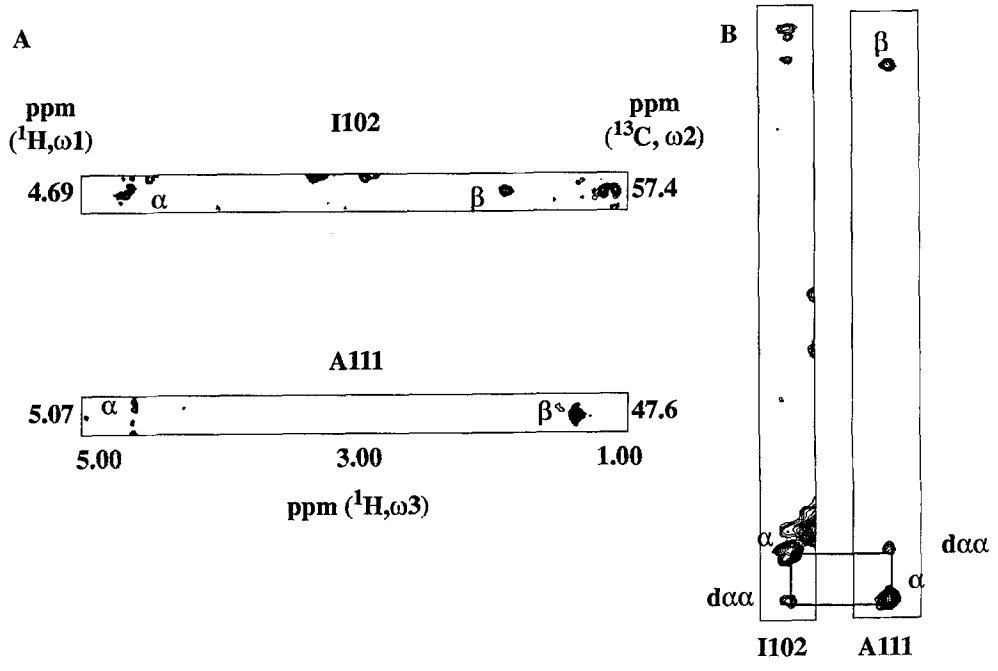

Fig. 6. Slices from (A) HCCH-TOCSY; and (B) NOESY-HSQC spectra of uniformly ^{15}N, ^{13}C-labeled ΔNZF1–3, illustrating the assignment of the $d_{\alpha\alpha}$ NOE connectivity between Ile^{102} and Ala^{111}.

eliminated by total exchange of ^1HN to ^2HN; it was established that exchange was complete by the lack of ^1H-^{15}N cross peaks in an overnight HSQC experiment.

A ^1H-^{13}C-correlated HSQC experiment is important for making the aromatic resonance assignments. The $C^\delta H$ and $C^\varepsilon H$ of tyrosine residues are not easily differentiated in homonuclear spectra. However, the $^{13}C^\varepsilon$ resonance of tyrosine has a unique chemical shift (about 116 ppm), which can be used to distinguish it from $C^\delta H$. The HSQC spectrum was also useful for assignment of the tryptophan side chain, because of the upfield chemical shift of $C^{\zeta 2}$ (about 113 ppm) which served as a starting point for tryptophan ring assignments.

A triple-resonance HCA(CO)N experiment was performed to minimize the ambiguities in backbone assignments of ΔNZF1–3. The HCA(CO)N experiment provides an independent method to link side-chain assignments to backbone assignments. Figure 5 illustrates the assignments of Phe^{301}, based on HCCH-COSY, HSQC and HCA(CO)N experiments. The 55.6 ppm $^{13}C^\alpha$ and 4.72 ppm $C^\alpha H$ resonances of Phe^{301} (Fig. 5A,C) are linked to the 117.2 ppm backbone ^{15}N resonance of Thr^{302} (Fig. 5B,C) via through-bond connectivity in the HCA(CO)N experiment. Due to the surprisingly long rotational correlation time (Liao and Wright, unpublished results) and the long delay required to transfer magnetization from ^{13}C of the carbonyl to ^{15}N ($^1J_{(CO)N}$ = 15 Hz) of the amide, some HCA(CO)N connectivities are missing in ZF1 and ZF2.

The assignments of ^1H, ^{15}N and ^{13}C resonances of ΔNZF1–3 are summarized in Table 1, which shows that nearly complete resonance assignments for ΔNZF1–3 have been achieved. Based on these assignments, NOE connectivities for each finger were determined.

The ^1H-^{13}C NOESY-HSQC spectrum was used to assign the NOEs important for secondary

TABLE 1
^{1}H, ^{13}C AND ^{15}N RESONANCE ASSIGNMENTS OF ΔNZF1–3[a]

Residue	HN	NH	H^{α}	C^{α}	H^{β}	C^{β}	H^{γ}	C^{γ}	Other
Met[98]			3.99	52.5	2.06	31.2	2.50	28.8	
Lys[99]			4.18	53.7	1.61/1.53	30.3	1.23	22.1	1.37 (H^{δ}); 2.90 (H^{ε}); 26.3 (C^{δ}); 39.7 (C^{ε})
Arg[100]	7.97	120.5	4.31	53.1	1.48/1.45	29.4	1.30	24.5	3.00 (H^{δ}); 40.3 (C^{δ})
Tyr[101]	8.55	122.1	4.35	54.9	2.94/2.67	36.1			6.94 (H^{δ}); 6.77 (H^{ε}); 131.4 (C^{δ}); 116.1 (C^{ε})
Ile[102]	8.33	124.4	4.68	57.4	1.63	37.9	1.34/0.91	25.1	0.74 (H^{δ}); 0.85 (H^{ε}); 10.5 (C^{δ}); 14.8 (C^{ε})
Cys[103]	9.00	129.5	4.20	59.8	2.91/3.10	27.6			
Ser[104]	7.87	122.5	4.41	56.2	3.96/3.84	61.6			
Phe[105]	9.18	126.6	4.11	57.4	2.83/2.70	36.1			7.01 (H^{δ}); 7.16 (H^{ε}); 7.01 (H^{ζ}); 129.4 (C^{δ}); 128.2 (C^{ε})
Ala[106]	8.55	128.7	3.98	51.9	1.28	16.0			
Asp[107]	8.69	115.4	4.34	52.5	2.83	37.3			
Cys[108]	7.77	121.2	4.53	58.6	3.29/3.02	27.6			
Gly[109]	8.35	104.8	3.93/3.80	42.8					
Ala[110]	8.16	125.9	3.83	51.3	0.85	16.6			
Ala[111]	7.33	121.3	5.06	48.3	1.08	20.3			
Tyr[112]	8.74	116.8	4.85	54.3	3.06/2.49	42.2			6.87 (H^{δ}); 6.33 (H^{ε}); 131.2 (C^{δ}); 115.7 (C^{ε})
Asn[113]			5.15	50.7	3.26/2.87	36.1			
Lys[114]	6.63	115.1	4.60	50.7	1.44/0.74	34.3	1.48/1.40	21.5	2.03/1.76 (H^{δ}); 3.11/3.04 (H^{ε}); 26.3 (C^{δ}); 39.7 (C^{ε})
Asn[115]			3.54	53.7	2.56/2.15	35.5			7.42/6.85 (H^{δ}); 113.0 (N^{δ})
Trp[116]		117.1	4.27	57.4	3.18/3.41	24.5			7.49 (C^{δ}); 10.49 (HN^{ε}); 7.49 ($H^{\zeta 2}$); 7.23 (H^{η}); 7.06 (H^{ε}); 7.28 ($H^{\zeta 3}$); 126.2 (H^{δ}); 124.5 (N^{ε}); 113.2 ($C^{\zeta 2}$); 122.7 ($C^{\eta 2}$); 120.6 ($C^{\varepsilon 3}$); 119.2 ($C^{\zeta 3}$)
Lys[117]	5.76	121.7	3.34	56.2	1.14/1.59	29.4	−0.51/−0.22	21.5	1.58/1.31 (H^{δ}); 2.87/2.57 (H^{ε}); 27.6 (C^{δ}); 39.7 (C^{ε})
Leu[118]	6.59	120.5	3.81	54.9	1.34/2.07	37.3	1.62	25.1	1.06/1.07 (H^{δ}); 23.3/19.2 (C^{δ})
Gln[119]	8.39	117.0	3.87	56.2	2.17/2.00	25.1	2.37	30.6	7.30/6.91 (H^{ε}); 113.0 (N^{ε})
Ala[120]	7.55	120.3	4.15	51.9	1.46	14.8			
His[121]	7.41	119.1	4.16	57.4	3.51/3.09	25.7			7.12 (H^{δ}); 7.49 (H^{ε}); 124.3 (C^{δ}); 136.1 (C^{ε})
Leu[122]	8.66	118.4	3.91	56.2	1.98/1.58	39.1	2.07	24.5	1.32/1.01 (H^{δ}); 22.1/23.3 (C^{δ})
Ser[123]	7.40	113.4	4.27	58.0	3.91	60.4			
Lys[124]	7.74	120.5	4.03	54.9	1.50	29.4	1.25/1.37	22.1	1.52 (H^{δ}); 2.88 (H^{ε}); 26.3 (C^{δ}); 39.7 (C^{ε})
His[125]	7.19	116.5	4.26	53.7	2.72/2.23	25.7			6.30 (H^{δ}); 7.83 (H^{ε}); 125.1 (C^{δ}); 137.0 (C^{ε})
Thr[126]	7.43	111.3	4.37	59.8	4.28	67.1	1.19	19.1	
Gly[127]	8.26	109.9	3.96/3.85	42.7					
Glu[128]	8.00	119.4	4.15	54.3	2.00/1.86	27.6	2.17	33.6	
Lys[129]	8.15	120.3	4.38	51.3	1.43/1.62	30.3	1.01	20.1	1.44/1.28 (H^{δ}); 2.80 (H^{ε}); 26.3 (C^{δ}); 39.7 (C^{ε})
Pro[130]			4.25	61.6	1.85/1.40	29.4	1.90/1.64	24.5	3.70/3.53 (H^{δ}); 48.3 (C^{δ})
Phe[201]	7.68	115.3	4.95	52.5	2.95/2.74	37.3			7.12 (H^{δ}); 7.34 (H^{ε})
Pro[202]			4.74	59.8	2.04/1.71	29.7			3.52/3.25 (H^{δ}); 48.3 (C^{δ})

TABLE 1
(continued)

Residue	HN	NH	H^{α}	C^{α}	H^{β}	C^{β}	H^{γ}	C^{γ}	Other
Cys^{203}	8.51	122.1	4.45	58.6	3.15/2.83	27.6			
Lys^{204}	8.57	127.0	4.37	53.7	1.95/1.75	30.0	1.44/1.25	22.1	1.56/1.42 (H^{δ}); 2.93 (H^{ϵ}); 26.3 (C^{δ}); 39.1 (C^{ϵ})
Glu^{205}	8.75	124.7	4.02	53.7	1.55/1.45	25.1	1.51/1.38	31.8	
Glu^{206}	8.72	127.0	3.99	56.2	2.00/1.95	26.6	2.26	33.6	
Gly^{207}	8.92	113.8	4.17/3.73	43.7					
Cys^{208}	7.80	123.3	4.50	58.0	3.18/2.65	27.6			
Glu^{209}	8.90	122.3	4.48	53.1	2.18/1.89	26.3	2.22/2.12	33.3	
Lys^{210}	8.00	121.4	4.13	53.7	1.45/1.42	31.2	1.54/1.48	23.9	1.63 (H^{δ}); 2.99 (H^{ϵ}); 28.2 (C^{δ}); 40.3 (C^{ϵ})
Gly^{211}	7.48	106.3	3.50/4.49	42.2					
Phe^{212}	7.74	116.2	4.98	54.9	3.56/2.99	41.6			7.41 (H^{δ}); 6.89 (H^{ϵ}); 6.28 (H^{ζ}); 129.0 (C^{δ}); 129.4 (C^{ϵ})
Thr^{213}	9.32	110.0	4.47	60.4	4.59	67.1	1.36	19.7	
Ser^{214}	7.10	113.3	4.52	53.7	3.82/3.68	64.2			
Leu^{215}	8.26	125.2	3.41	54.3	1.37/1.04	38.5	1.25	23.9	0.77/0.88 (H^{δ}); 22.7/20.9 (C^{δ})
His^{216}			4.22	56.8	2.99/2.83	26.9			6.56 (H^{δ}); 7.69 (H^{ϵ}); 117.1 (C^{δ}); 136.5 (C^{ϵ})
His^{217}	7.40	117.9	4.15	56.2	3.11	28.8			6.91 (H^{δ}); 7.85 (H^{ϵ}); 115.3 (C^{δ}); 136.7 (C^{ϵ})
Leu^{218}	7.29	122.1	3.49	56.1	2.07/1.60	37.9	1.62	25.1	1.10/1.06 (H^{δ}); 23.9/19.7 (C^{δ})
Thr^{219}	8.83	116.9	3.76	64.1	4.16	65.3	1.15	18.5	
Arg^{220}	7.53	120.7	3.94	56.8	1.72	26.9	1.55/1.49	23.9	3.06 (H^{δ}); 40.3 (C^{δ})
His^{221}	7.61	118.9	4.27	56.8	3.05/2.74	26.3			7.10 (H^{δ}); 7.92 (H^{ϵ}); 125.5 (C^{δ}); 137.6 (C^{ϵ})
Ser^{222}	9.01	118.5	4.04	60.4	3.91	61.0			
Leu^{223}	7.05	120.4	4.15	54.3	1.77/1.54	39.1	1.83	24.2	0.88/0.81 (H^{δ}); 23.9/19.7 (C^{δ})
Thr^{224}	7.85	109.5	4.14	61.0	4.03	66.5	1.16	17.8	
His^{225}	7.16	119.2	4.78	53.1	3.12	25.7			6.52 (H^{δ}); 8.04 (H^{ϵ}); 125.3 (C^{δ}); 137.7 (C^{ϵ})
Thr^{226}	7.75	112.8	4.31	59.2	4.18	67.1	1.15	19.1	
Gly^{227}	8.32	110.6	3.96/3.95	42.7					
Glu^{228}	8.12	120.3	4.18	54.3	1.98/1.91	27.6	2.21	33.6	
Lys^{229}	8.32	122.6	4.22	53.7	1.61/1.48	30.0	1.28/1.15	22.1	1.52 (H^{δ}); 2.87/2.83 (H^{ϵ}); 26.9 (C^{δ}); 39.1 (C^{ϵ})
Asn^{230}	8.10	118.8	4.68	50.7	2.50/2.40	37.9			7.30/6.86 (H^{δ}); 112.3 (N^{δ})
Phe^{301}	8.54	118.7	4.68	55.6	2.94/2.73	36.7			7.18 (H^{δ}); 7.42 (H^{ϵ}); 129.4 (C^{δ})
Thr^{302}	8.46	117.4	4.77	58.6	4.20	67.1	1.20	19.1	
Cys^{303}	8.66	125.3	4.29	59.2	3.10	26.9			
Asp^{304}	7.35	127.1	4.59	53.7	2.53/2.10	39.7			
Ser^{305}	9.16	118.8	4.34	56.2	3.44/2.98	60.4			
Asp^{306}	8.66	128.7	4.39	53.7	2.62	37.9			
Gly^{307}	8.63	112.3	4.09/3.80	42.8					
Cys^{308}	7.77	123.6	4.52	56.8	3.21/2.78	28.2			
Asp^{309}	8.66	126.3	4.87	51.3	2.72/2.60	39.1			
Leu^{310}	7.80	122.4	3.99	53.7	1.42/0.94	40.3	1.68	25.1	0.70/0.69 (H^{δ}); 23.3/20.3 (C^{δ})
Arg^{311}	7.53	117.0	5.06	51.3	1.55/1.37	31.2	1.53/1.41	25.1	3.05 (H^{δ}); 41.0 (C^{δ})

TABLE 1 (continued)

Residue	HN	NH	H^{α}	C^{α}	H^{β}	C^{β}	H^{γ}	C^{γ}	Other
Phe^{312}	8.67	116.2	4.83	54.3	3.35/2.65	42.2			7.14 (H^{δ}); 6.91 (H^{ε}); 5.91 (H^{ζ}); 129.0 (C^{δ}); 128.6 (C^{ε}); 127.4 (C^{ζ})
Thr^{313}	9.38	111.7	4.61	61.6	4.48	67.1	1.37	20.3	
Thr^{314}	7.16	107.0	4.59	56.2	4.41	70.8	1.25	19.1	
Lys^{315}	8.16	124.0	3.20	56.8	1.47/1.21	29.4	1.15/1.09	22.7	1.59 (H^{δ}); 2.88 (H^{ε}); 26.9 (C^{δ}); 39.7 (C^{ε})
Ala^{316}	8.30	120.1	3.95	52.5	1.31	15.4			
Asn^{317}	7.97	117.5	4.43	53.1	2.91	34.9			
Met^{318}	7.44	123.6	2.34	57.4	2.32/1.67	27.6	2.66/2.16	30.6	2.08 (H^{ε}); 14.2 (C^{ε})
Lys^{319}	8.55	120.1	3.93	56.2	1.86/1.82	28.9	1.43/1.49	22.1	1.53 (H^{δ}); 2.83/2.77 (H^{ε}); 25.1 (C^{δ}); 39.1 (C^{ε})
Lys^{320}	7.83	120.0	4.07	57.4	1.90	30.0	1.61/1.45	22.7	1.72 (H^{δ}); 2.96 (H^{ε}); 26.9 (C^{δ}); 39.7 (C^{ε})
His^{321}	7.21	119.1	4.48	56.8	3.13	25.1			7.54 (H^{δ}); 7.50 (H^{ε}); 124.3 (C^{δ}); 137.1 (C^{ε})
Phe^{322}	9.39	123.2	3.82	59.8	3.44/3.33	37.3			7.34 (H^{δ})
Asn^{323}	8.55	115.9	4.47	53.1	2.84	35.5			7.51/6.92 (H^{δ}); 111.3 (N^{δ})
Arg^{324}	7.30	116.9	4.07	55.6	1.51/1.68	28.8	1.18/0.93	23.9	2.96 (H^{δ}); 40.3 (C^{δ})
Phe^{325}	7.86	114.0	4.25	57.4	2.26/1.62	37.3			7.06 (H^{δ}); 7.39 (H^{ε}); 7.32 (H^{ζ})
His^{326}	7.73	115.3	4.92	51.3	2.73/1.78	25.7			6.51 (H^{δ}); 8.02 (H^{ε}); 126.4 (C^{δ}); 137.1 (C^{ε})
Asn^{327}	7.58	118.4	4.69	50.7	2.89/2.59	36.7			7.45/6.79 (H^{δ}); 111.7 (N^{δ})
Ile^{328}	7.87	120.5	4.13	58.6	1.82	36.1	1.07/1.34	24.5	0.83 (H^{δ}); 0.85 (H^{ε}); 9.93 (C^{δ}); 14.5 (C^{ε})
Lys^{329}	7.89	130.4	4.13	55.6	1.78/1.63	31.2	1.35	22.1	1.63 (H^{δ}); 2.99 (H^{ε}); 26.3 (C^{δ}); 39.7 (C^{ε})

[a] Experimental conditions: 300 K, pH 6.5.

and tertiary structure determination. The observed $d_{\alpha\beta}(i,i+3)$ NOE connectivities are characteristic of a helix and strong long-range $d_{\alpha\alpha}$ connectivities suggest a β-sheet structure. Figure 6 illustrates the determination of $d_{\alpha\alpha}$ backbone NOEs between Ile^{102} and Ala^{111}. Figure 6A contains slices from the HCCH-TOCSY and Fig. 6B contains slices from the ^{1}H-^{13}C-correlated NOESY-HSQC experiment, showing a $d_{\alpha\alpha}$ NOE connectivity between Ile^{102} and Ala^{111}. In addition, a 4D ^{13}C-edited NOESY spectrum was used to further improve spectral resolution. Since NOE donor protons are labeled with the directly attached ^{13}C frequencies in the 4D HMQC-NOESY-HMQC experiment, the severe overlap in the F_1 dimension is reduced. Figure 7 illustrates overlapped peaks at 57.4 ppm in the 3D spectrum, that are separated in the 4D experiment.

Measurement of $^{3}J_{HN\alpha}$ coupling constants is crucial for defining the polypeptide backbone dihedral angles. Due to the large line widths which cause cancellation of antiphase cross peaks, homonuclear methods could not be used to measure coupling constants for ΔNZF1–3. Instead, the J-modulated HSQC experiment was performed to extract $^{3}J_{HN\alpha}$ values. Coupling constants resulting from curve fitting were divided into two categories ($^{3}J_{HN\alpha} > 7$ Hz, or $^{3}J_{HN\alpha} < 4$ Hz), as shown in Fig. 8.

Secondary and tertiary structure

The NOE connectivities of ΔNZF1–3 are summarized in Fig. 8. The NOE intensities varied

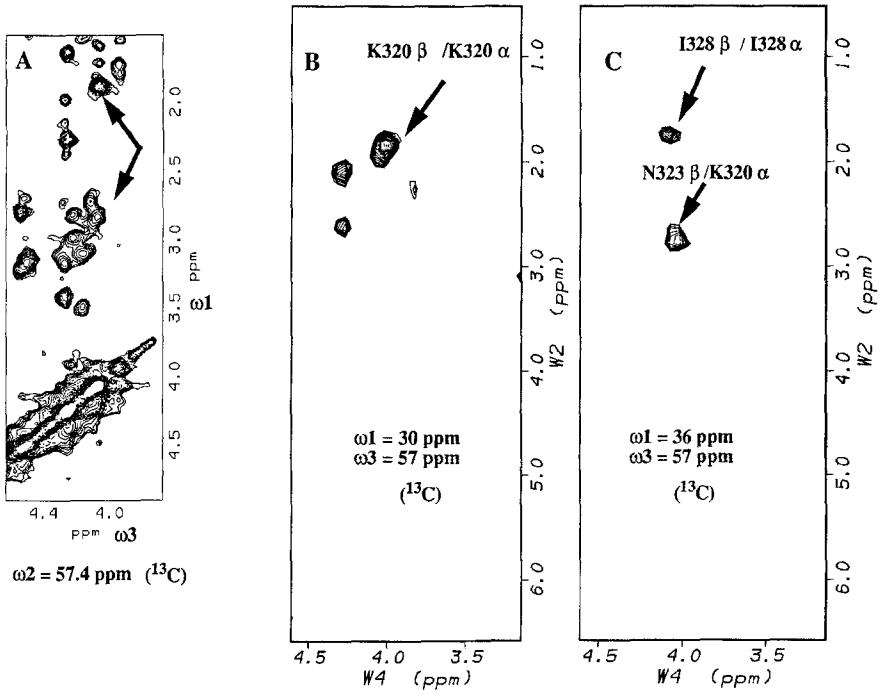

Fig. 7. Slices from (A) 3D NOESY-HSQC; and (B,C) 4D HMQC-NOESY-HMQC spectra of uniformly ^{15}N, ^{13}C-labeled ΔNZF1–3, illustrating the improved resolution on going from three to four dimensions.

between the fingers (ZF3 > ZF1 > ZF2), due to different rotational correlation times for the individual fingers (Liao et al., unpublished results). Therefore, the relative NOE intensities were calibrated separately for each finger. Since ZF2 has the longest apparent rotational correlation time and the lowest signal intensities in the three fingers, some expected NOE connectivities in ZF2 are missing. Based on sequential, medium-range and long-range NOE connectivities, each finger clearly folds into the characteristic β-sheet-helix structure motif.

The strong $d_{\alpha N}(i,i+1)$ NOE connectivities, and long-range $d_{\alpha\alpha}(x02,x11)$, $d_{NN}(x01,x12)$, $d_{\alpha N}(x11,x03)$, $d_{\alpha N}(x02,x12)$ and $d_{NN}(x03,x10)$ (where x = 1 or 3 for fingers 1 and 3, respectively) NOE connectivities and the large $^3J_{HN\alpha}$ coupling constants observed for ZF1 and ZF3 indicate that the first 12 residues in each finger form a β-hairpin (Fig. 9A). Weak long-range $d_{N\alpha}(203,211)$, $d_{NN}(203,210)$, $d_{\alpha\alpha}(202,211)$ and $d_{\delta\alpha}(130,213)$ NOE connectivities, combined with large $^3J_{HN\alpha}$ coupling constants, also suggest that β-sheet structure is present in ZF2. Since the $d_{\alpha\alpha}(202,211)$ NOE is very weak and a weak NOE connectivity between amide protons of Cys^{203} and Phe^{215} is observed (Fig. 9B), the sheet structure appears to be distorted, presumably due to the presence of Pro^{202}. NOE connectivities have also been observed between β-protons of the first conserved cysteine ligand at position 3 and β-protons of residues at position 10 of each finger (Fig. 9). Since all these β-protons presumably point outward, the unusual NOE connectivities plus the small $^3J_{HN\alpha}$ of Cx03 (x = 1, 2, 3) suggest twisting in the middle of the β-sheets, which is likely caused by zinc coordination.

The number of NOE connectivities observed for residues 113-114 in ZF1, 213-214 in ZF2 and

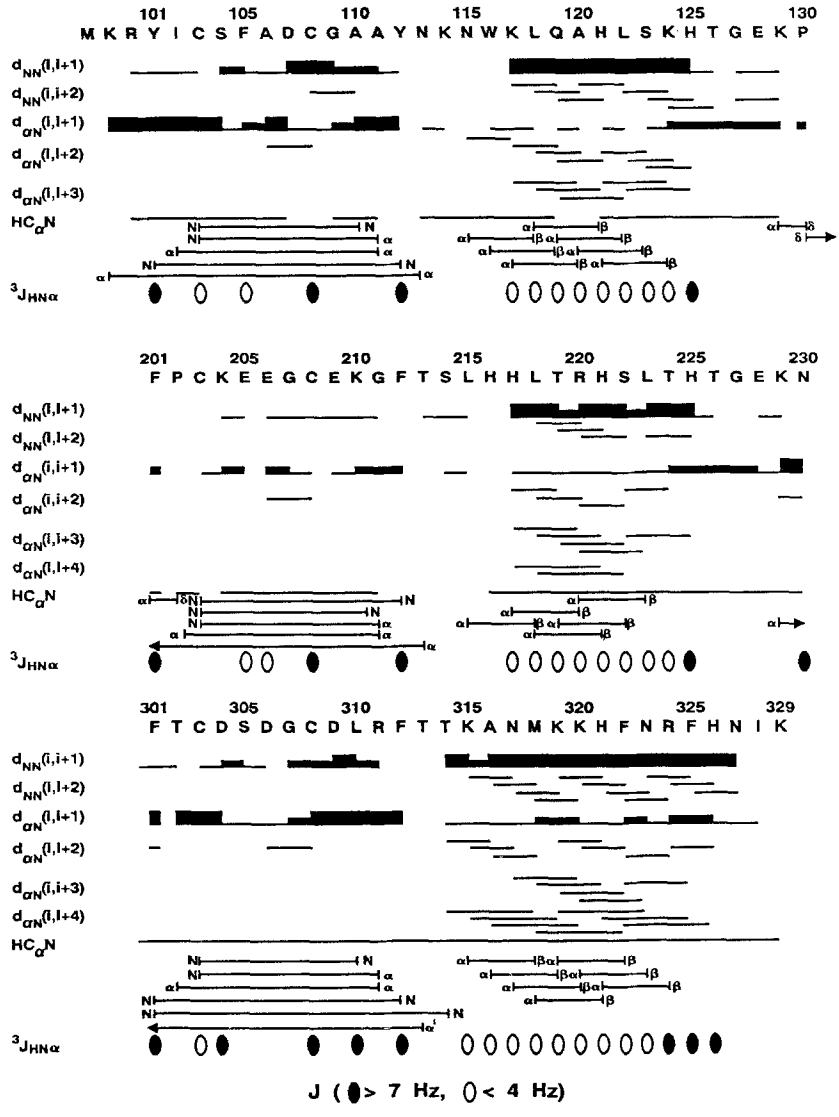

Fig. 8. Summary of the backbone NOE connectivities, $HC^{\alpha}N$ through-bond connectivities and $^{3}J_{HN\alpha}$ coupling constants for ΔNZF1–3. The NOE connectivities involving NH are indicated by bars and lines between the residues. The height of the bars gives a qualitative measure of the relative strength of the NOE in the 140-ms 3D ^{1}H-^{15}N NOESY-HSQC spectrum. The NOE intensities were calibrated for each finger separately. The $d_{\alpha\alpha}$, $d_{\alpha\beta}(i,i+3)$ sequential NOEs and NOEs involving the $C^{\delta}H$ of prolines were observed in a 100-ms 3D ^{1}H-^{13}C NOESY-HSQC spectrum. The $^{3}J_{HN\alpha}$ coupling constants were measured according to the technique outlined in the Materials and Methods section. Open ovals represent a $^{3}J_{HN\alpha}$ coupling constant smaller than 3 Hz and dark ovals represent a $^{3}J_{HN\alpha}$ coupling constant larger than 7 Hz.

313-314 in ZF3 drops significantly (Fig. 8). This is the region previously described as the fingertip (Lee et al., 1989). Immediately following the fingertip region, a new pattern of NOE connectivities characteristic of α-helix is observed. Extensive medium-range NOE connectivities are observed for residues 115–125 (ZF1) and 215–225 (ZF2). Small $^{3}J_{HN\alpha}$ coupling constants (< 4 Hz) through-

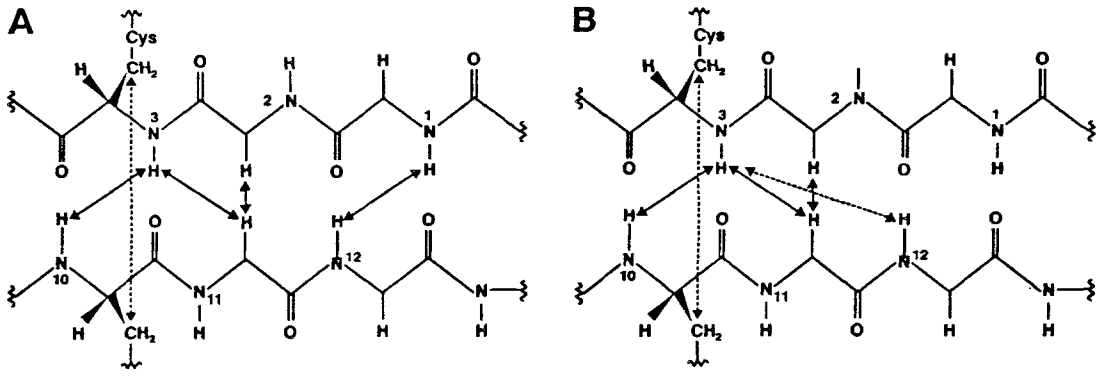

Fig. 9. Characteristic NOE connectivities observed in the β-sheet in each finger. The dashed lines indicate NOE connectivities that are not normally observed in regular β-sheet structures. (A) ZF1 and ZF3; (B) ZF2.

out both regions are consistent with a helical conformation. However, the $^3J_{HN\alpha}$ coupling constants of His[125] and His[225] are larger than 7 Hz, suggesting that these residues do not form part of the helix. This is probably the result of zinc coordination of His[125] and His[225]. The folding of amino acids 314–326 in ZF3 is more complicated. Strong $d_{NN}(i,i+1)$ NOE connectivities and $d_{NN}(i,i+2)$, $d_{\alpha N}(i,i+1)$, $d_{\alpha N}(i,i+2)$, $d_{\alpha N}(i,i+3)$ and $d_{\alpha N}(i,i+4)$ NOE connectivities are observed for residues 314 to 326, suggesting helical structure in Thr[314]–His[326]. However, no $d_{\alpha\beta}(i,i+3)$ NOE connectivities are observed between Phe[322] and Phe[325] or between Asn[323] and His[326]. Also, the $^3J_{HN\alpha}$ coupling constants of Arg[324], Phe[325] and His[326] are around 7 Hz, which is outside the range of an α-helix. Thus, the helical structure in ZF3 appears to be distorted from Arg[324] to His[326]. This distortion is caused by zinc coordination, since four residues are flanked by the two conserved histidines in ZF3, instead of three residues as in ZF1 and ZF2. A similar distortion has also been observed in a ZFY zinc finger containing four amino acids between the histidine ligands (Kochoyan et al., 1991a).

Strong $d_{\alpha N}(i,i+1)$ and weak $d_{NN}(i,i+1)$ values are observed for the sequences linking ZF1, ZF2 and ZF3, suggesting that they adopt an extended structure. Measurements of backbone ^{15}N relaxation data show slightly decreased S^2 values for both linkers (Liao and Wright, unpublished results), suggesting that the linker backbone has some flexibility.

Backbone chemical shifts also provide information on secondary structure. An empirical correlation between $^{13}C^\alpha$ chemical shifts and secondary structure has been established recently (Spera and Bax, 1991; Wishart et al., 1991). A systematic downfield shift occurs for $^{13}C^\alpha$ in helical regions (2.3 ppm average observed by Spera and Bax (1991) and 3.1 ppm average observed by Wishart et al. (1991)) and an upfield secondary shift is observed for $^{13}C^\alpha$ in β-strand and extended structures (−1.5 ppm average observed by Spera and Bax (1991) and −1.3 ppm average observed by Wishart et al. (1991)). The $^{13}C^\alpha$ chemical shift differences between ΔNZF1–3 and random coil values (Howarth and Lilley, 1978; Richarz and Wüthrich, 1978) are shown in Fig. 10. For each zinc finger, the $^{13}C^\alpha$ resonances for residues x15 to x25 (x = 1, 2 or 3) are shifted substantially downfield, indicating the presence of helix. The helical regions indicated by the chemical shift data are in excellent agreement with those identified from medium-range NOE connectivities. For ZF3, both the NOEs and the $^{13}C^\alpha$ chemical shifts suggest that the helix extends from Lys[315] to

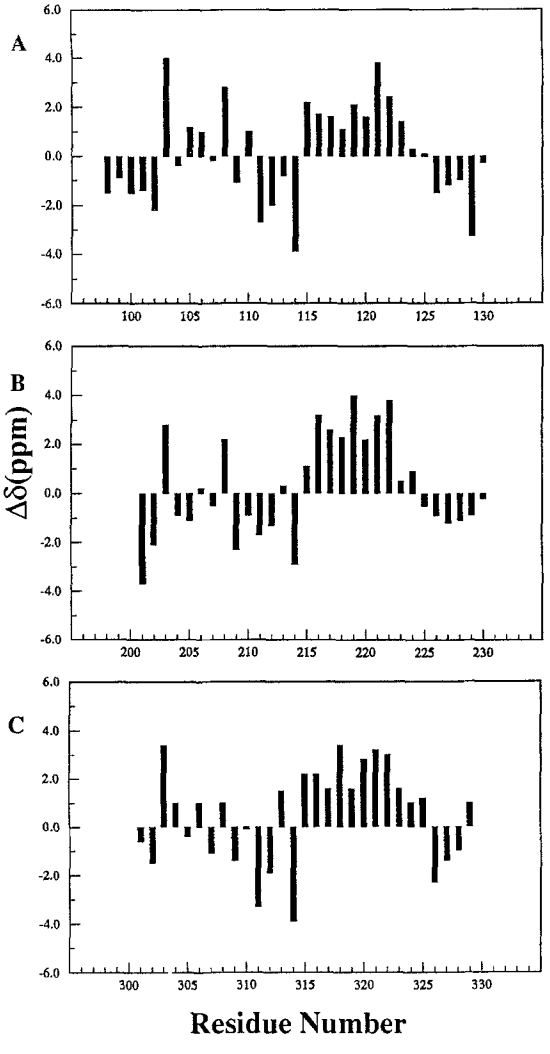

Fig. 10. Plot of the differences between the $^{13}C^{\alpha}$ chemical shift and the random coil shift (Richarz and Wüthrich, 1978) versus the residue number of ΔNZF1–3. (A) ZF1; (B) ZF2; and (C) ZF3.

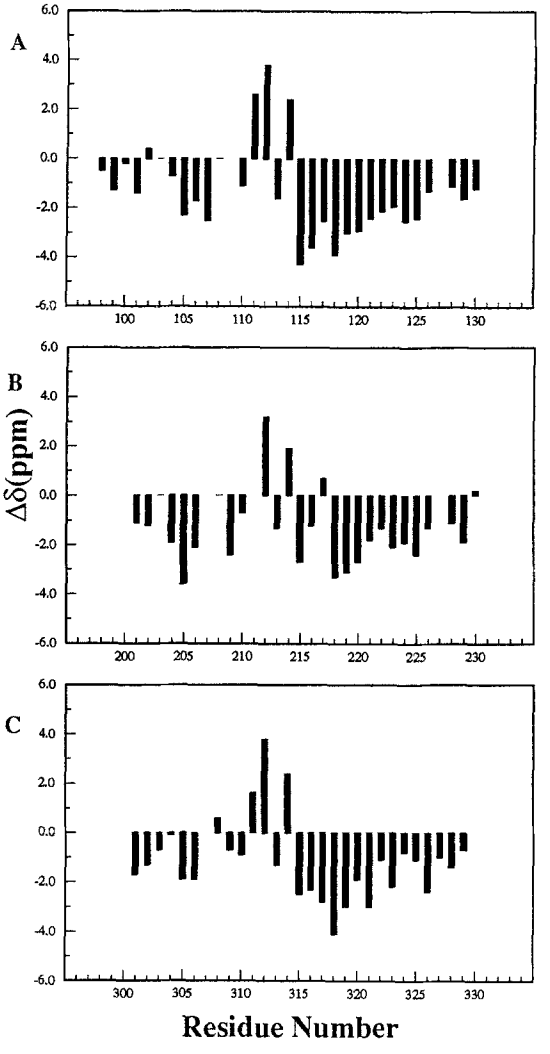

Fig. 11. Plot of the differences between the $^{13}C^{\beta}$ chemical shift and the random coil shift (Richarz and Wüthrich, 1978) versus the residue number of ΔNZF1–3. (A) ZF1; (B) ZF2; and (C) ZF3.

Phe^{325}. The average secondary shifts are 1.8 ppm for Asn^{115} through Lys^{124}, 2.4 ppm for Leu^{215} through Thr^{224} and 2.5 ppm for Lys^{315} through Phe^{325}. These values are close to the average $^{13}C^{\alpha}$ secondary shifts for helices published previously (Spera and Bax, 1991; Wishart et al., 1991). The linker regions show upfield secondary shifts (−1.2 ppm average) which support the extended conformation suggested by the pattern of NOE connectivities. The $^{13}C^{\alpha}$ chemical shift differences are more complicated for residues 1–12 in each finger. Based on the NOE connectivities, these three sequences form β-strand structures. However, mixed secondary shifts are observed; especially notable are the downfield shifts for the cysteine ligands, which are caused by zinc coordination. If the secondary shifts for cysteine are excluded, the average shifts are −0.9, −1.4 and

−0.8 ppm for residues x01–x12 of ZF1, ZF2 and ZF3, respectively. These values support the previous conclusion that β-sheet conformations are formed in these regions.

The $^{13}C^{\beta}$ chemical shift differences between ΔNZF1–3 and random coil values (Howarth and Lilley, 1978; Richarz and Wüthrich, 1978) are shown in Fig. 11; generally, upfield secondary chemical shifts are observed. Most of the downfield secondary chemical shifts are located in the region between residues 11 and 14 in each finger, which is the fingertip.

Conserved patterns of proton chemical shifts have been identified previously and serve as a fingerprint for a correctly folded zinc finger (Lee et al., 1992a,b). Table 2 lists the ^{1}H chemical shifts and secondary chemical shifts (Bundi and Wüthrich, 1979) of several diagnostic backbone and side-chain proton resonances of zinc fingers from TFIIIA. In all cases secondary shifts characteristic of folded zinc fingers are observed. The shift patterns suggest similar folded structures for each of the TFIIIA zinc fingers. An unusually large upfield shift is observed for the $C^{\alpha}H$ resonance of Met^{318}, which is probably caused by the ring currents of Phe^{322} and Phe^{325}.

A large downfield shift (of the order of 8 ppm) is observed for the $^{13}C^{\delta}$ resonances of the histidine ligands and is diagnostic of zinc coordination. Similar shifts have been observed for an Xfin zinc finger (Lee et al., 1992).

Many long-range NOE connectivities involving side chains are observed between the β-sheet and helix in each finger (Fig. 12). These NOE connectivities confirm the tight packing between sheet and helix (Lee et al., 1989; Omichinski et al., 1990,1992; Klevit et al., 1991; Kochoyan et al., 1991a,b). ZF1, ZF2 and ZF3 all fold into the canonical zinc finger conformation, with the aromatic ring of residue x12 and the side chain of residue x18 in each finger providing the important hydrophobic packing. Residue 318 is a methionine in ZF3, instead of the more usual

TABLE 2
KEY CONSERVED ^{1}H CHEMICAL SHIFTS FOR SEVERAL TFIIIA ZINC FINGERS

	7NH	11C$^{\alpha}$H	15C$^{\alpha}$H	18NH	18C$^{\alpha}$H	25NH[a]	25C$^{\alpha}$H[a]	F12$^{\zeta}$H	H25$^{\delta}$H[a]
ZF1[b]	8.69	5.06	3.54	6.59	3.81	7.19	4.26	[c]	6.30
	(0.28)	(0.71)	(−1.21)	(−1.83)	(−0.57)	(−1.22)	(−0.37)		(−0.84)
ZF2[b]	8.92	4.49[d]	3.41	7.29	3.49	7.16	4.78	6.28	6.52
	(0.53)	(0.52)	(−0.97)	(−1.13)	(−0.88)	(−1.25)	(0.15)	(−1.06)	(−0.62)
ZF3[b]	8.63	5.06	3.20	7.44	2.34	7.73	4.92	5.91	6.51
	(0.24)	(0.68)	(−1.16)	(−0.98)	(−2.18)	(−0.68)	(0.29)	(−1.43)	(−0.63)
ZF2[e,f]	9.12	4.43[d]	3.37	7.53	3.57	7.04	4.45	6.24	6.47
	(0.73)	(0.46)	(−1.01)	(−0.89)	(−0.80)	(−1.37)	(0.11)	(−1.10)	(−0.67)
ZF5[f,g]	9.07	4.94	3.55	6.99	3.32	7.12	4.62	6.41	6.31
	(0.68)	(0.56)	(−0.89)	(−1.43)	(−1.06)	(−1.29)	(0.18)	(−0.93)	(0.83)

The values in parentheses represent chemical shift differences (experimental – random coil).

[a] For ZF3, these values should be 26NH, 26C$^{\alpha}$H and H26$^{\eta}$H.

[b] Experimental conditions: 300 K, pH 6.5.

[c] Phe^{12} is replaced by Tyr^{12}.

[d] The residue at this position for ZF2 is glycine. Chemical shift data for the most downfield proton are shown.

[e] Experimental conditions: 278 K, pH 6.5.

[f] Both are chemically synthesized single-finger peptides (Lee et al., 1992b).

[g] Experimental conditions: 278 K, pH 5.5.

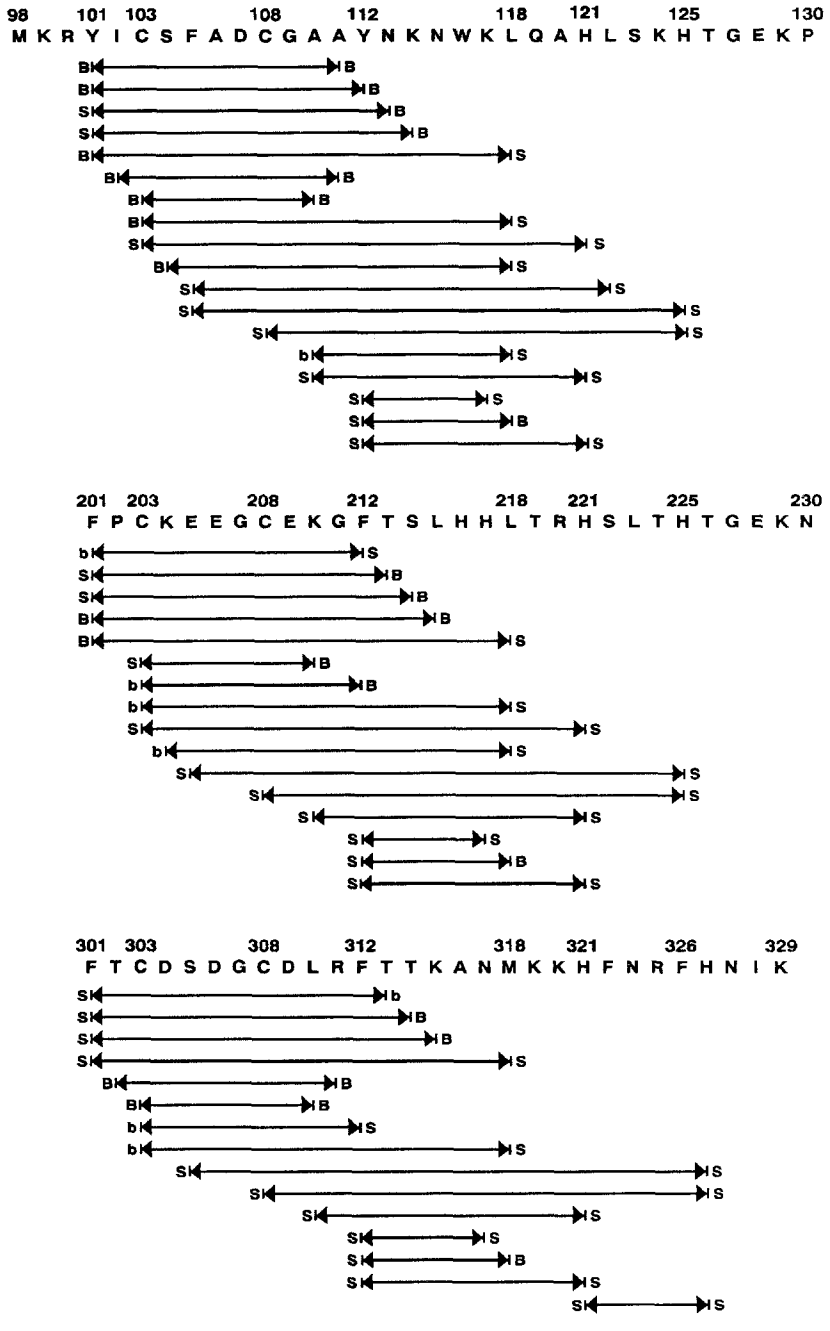

Fig. 12. Summary of side-chain NOE connectivities in each finger of ΔNZF1–3. b = backbone, s = side chain and B = backbone and side chain.

leucine. The NOE connectivities involving Met^{318} in ZF3 are very similar to those observed for Leu^{218} and Leu^{118} in ZF2 and ZF1, respectively. Clearly the methionine at position 18 can participate fully in the hydrophobic packing of the core of the zinc finger.

CONCLUSIONS

Nearly complete resonance assignments for a protein containing the first three zinc fingers of TFIIIA have been achieved, using a combination of single-, double- and triple-resonance multi-dimensional NMR experiments. The assignments represent the first step toward determination of the solution structures and dynamics of the polypeptide. Based on the observed pattern of medium- and long-range NOE connectivities, $^3J_{HN\alpha}$ coupling constants and conserved chemical shifts, each finger of ΔNZF1–3 adopts the canonical structure of β-sheet, followed by helix. The β-sheet of ZF2 is not disrupted by Pro^{202}. Distortions are apparent in the helix of finger 3. The linker sequences adopt a more extended structure. Calculation of the 3D solution structure of ΔNZF1–3 is currently in progress and determination of the structure of the complex with DNA is being undertaken.

ACKNOWLEDGEMENTS

We thank Dr. Mark Rance for expert advice on NMR experiments and Dr. Joel Gottesfeld for valuable discussions. This work was supported by grant GM36643 from the National Institutes of Health. X.L. acknowledges the Cancer Research Institute/Miriam and Benedict Wolf Fellowship for support. K.C. acknowledges receipt of NIH postdoctoral award F32 CA09023.

REFERENCES

Bax, A. and Subramanian, S.J. (1986) *J. Magn. Reson.*, **67**, 565–569.
Bax, A. (1989) *Annu. Rev. Biochem.*, **58**, 223–256.
Bax, A., Ikura, M., Kay, L.E., Torchia, D. and Tschudin, R. (1990a) *J. Magn. Reson.*, **86**, 304–318.
Bax, A., Clore, G.M. and Gronenborn, A.M. (1990b) *J. Magn. Reson.*, **88**, 425–431.
Bodenhausen, G. and Ruben, D.J. (1980) *Chem. Phys. Lett.*, **69**, 185–187.
Braunschweiler, L. and Ernst, R.R. (1983) *J. Magn. Reson.*, **53**, 521–526.
Braunschweiler, L., Bodenhausen, G. and Ernst, R.R. (1984) *Mol. Phys.*, **48**, 535–560.
Bundi, A. and Wüthrich, K. (1979) *Biopolymers*, **18**, 285–297.
Cavanagh, J. and Rance, M. (1990) *J. Magn. Reson.*, **88**, 72–76.
Clemens, K., Liao, X., Wolf, V., Wright, P.E. and Gottesfeld, J. (1992) *Proc. Natl. Acad. Sci. USA*, **89**, 10822–10826.
Clemens, K., Wolf, V., McBryant, S.J., Zhang, P., Liao, X., Wright, P.E. and Gottesfeld, J. (1993) *Science*, **260**, 530–533.
Clore, G.M. and Gronenborn, A.M. (1989) *Crit. Rev. Biochem. Mol. Biol.*, **24**, 479–564.
Clore, G.M., Kay, L.E., Bax, A. and Gronenborn, A.M. (1991) *Biochemistry*, **30**, 12–18.
El-Baradi, T. and Pieler, T. (1991) *Mech. Dev.*, **35**, 155–169.
Engelke, D.R., Ng, S.-Y., Shastry, B.S. and Roeder, R.G. (1980) *Cell*, **19**, 717–728.
Fesik, S.W. and Zuiderweg, E.R.P. (1990) *Q. Rev. Biophys.*, **23**, 97–131.
Ginsberg, A.M., King, B.O. and Roeder, R.G. (1984) *Cell*, **39**, 479–489.
Honda, B.M. and Roeder, R.G. (1980) *Cell*, **22**, 119–126.
Howarth, O.W. and Lilley, D.M.J. (1978) *Prog. NMR Spectrosc.*, **12**, 1–40.
Ikura, M., Kay, L.E. and Bax, A. (1991) *J. Biomol. NMR*, **1**, 299–304.
Jeener, J., Meier, B.H., Bachmann, P. and Ernst, R.R. (1979) *J. Chem. Phys.*, **71**, 4546–4553.
Klevit, R.E., Herriott, J.R. and Horvath, S. (1991) *Proteins*, **7**, 214–226.
Kochoyan, M., Havel, T.F., Nguyen, D.T., Dahl, C.E., Keutmann, H.T. and Weiss, M.A. (1991a) *Biochemistry*, **30**, 3371–3386.
Kochoyan, M., Keutmann, H.T. and Weiss, M.A. (1991b) *Biochemistry*, **30**, 7063–7072.
Lee, M.S., Gippert, G.P., Soman, K.V., Case, D.A. and Wright, P.E. (1989) *Science*, **245**, 635–637.

Lee, M.S., Palmer III, A.G. and Wright, P.E. (1992a) *J. Biomol. NMR*, **2**, 307–322.
Lee, M.S., Mortishire-Smith, R.J. and Wright, P.E. (1992b) *FEBS Lett.*, **309**, 29–32.
Liao, X., Clemens, K.R., Tennant, L., Wright, P.E. and Gottesfeld, J.M. (1992) *J. Mol. Biol.*, **223**, 857–871.
Live, D.H., Davis, D.G., Agosta, W.C. and Cowburn, D. (1984) *J. Am. Chem. Soc.*, **106**, 1939–1941.
Marion, D. and Wüthrich, K. (1983) *Biochem. Biophys. Res. Commun.*, **113**, 967–974.
Marion, D., Ikura, M., Tschudin, R. and Bax, A. (1989) *J. Magn. Reson.*, **85**, 393–399.
McIntosh, L.P. and Dahlquist, F.W. (1990) *Q. Rev. Biophys.*, **23**, 1–38.
Messerle, B.A., Wider, G., Otting, G., Weber, C. and Wüthrich, K. (1989) *J. Magn. Reson.*, **85**, 608–613.
Miller, J., McLachlan, A.D. and Klug, A. (1985) *EMBO J.*, **4**, 1609–1614.
Morris, G.A. and Freeman, R. (1979) *J. Am. Chem. Soc.*, **101**, 760–762.
Neri, D., Otting, G. and Wüthrich, K. (1990) *J. Am. Chem. Soc.*, **112**, 3663–3665.
Norwood, T.J., Boyd, J., Heritage, J.E., Soffe, N. and Campbell, I.D. (1990) *J. Magn. Reson.*, **87**, 488–501.
Omichinski, J.G., Clore, G.M., Appella, E., Sakaguchi, K. and Gronenborn, A.M. (1990) *Biochemistry*, **29**, 9324–9334.
Omichinski, J.G., Clore, G.M., Robien, M., Sakaguchi, K., Appella, E. and Gronenborn, A.M. (1992) *Biochemistry*, **31**, 3907–3917.
Palmer III, A.G., Cavanagh, J., Byrd, R.A. and Rance, M. (1991) *J. Magn. Reson.*, **96**, 416–424.
Palmer III, A.G., Fairbrother, W.J., Cavanagh, J., Wright, P.E. and Rance, M. (1992) *J. Biomol. NMR*, **2**, 103–108.
Pavletich, N.P. and Pabo, C.O. (1991) *Science*, **252**, 809–917.
Pelham, H.R. and Brown, D.D. (1980) *Proc. Natl. Acad. Sci. USA*, **77**, 4170–4174.
Richarz, R. and Wüthrich, K. (1970) *Biopolymers*, **17**, 2133–2141.
Rance, M. and Wright, P.E. (1986) *J. Magn. Reson.*, **66**, 372–378.
Sakonju, S., Bogenhagen, D.F. and Brown, D.D. (1980) *Cell*, **19**, 13–25.
Shaka, A.J., Barker, P.B. and Freeman, R. (1985) *J. Magn. Reson.*, **64**, 547–552.
Shaka, A.J., Lee, C.J. and Pines, A. (1988) *J. Magn. Reson.*, **77**, 274–293.
Smith, D.R., Jackson, I.J. and Brown, D.D. (1984) *Cell*, **37**, 645–652.
Spera, A.J. and Bax, A. (1991) *J. Am. Chem. Soc.*, **113**, 5490–5492.
Vrana, K.E., Churchill, M.E.A., Tullius, T.D. and Brown, D.D. (1988) *Mol. Cell. Biol.*, **8**, 1684–1696.
Wishart, D.S., Sykes, B.D. and Richards, F.M. (1991) *J. Mol. Biol.*, **222**, 311–333.
Wüthrich, K. (1986) *NMR of Proteins and Nucleic Acids*, Wiley, New York, NY.
Wüthrich, K. (1989) *Acc. Chem. Res.*, **22**, 36–44.